Analysis of mycobacterial infection-induced changes to host lipid metabolism in a zebrafish infection model reveals a conserved role for LDLR in infection susceptibility

Matt D. Johansen[1, 2], Elinor Hortle[2], Joshua Kasparian[1, 2], Alejandro Romero[3], Beatriz Novoa[3], Antonio Figueras[3], Warwick J. Britton[2, 4, 5], Kumudika de Silva[1, 5], Auriol C. Purdie[1, 5], Stefan H. Oehlers[2, 4, 5 *]

[1] Sydney School of Veterinary Science, Faculty of Science, The University of Sydney, Camden, NSW, Australia

[2] Tuberculosis Research Program, Centenary Institute, University of Sydney, Camperdown, NSW, Australia

[3] Institute of Marine Research (IIM), Spanish National Research Council (CSIC), Vigo, Spain

[4] Sydney Medical School, The University of Sydney, Newtown, NSW, Australia

[5] Marie Bashir Institute, The University of Sydney, Newtown, NSW, Australia

[*] Corresponding author: stefan.oehlers@sydney.edu.au

Abstract

Host lipid metabolism is an important target for subversion by pathogenic mycobacteria such as *Mycobacterium tuberculosis*. Systemic dyslipidemia and the appearance of foam cells within the granuloma are well-characterised effects of chronic tuberculosis. The zebrafish-*Mycobacterium marinum* infection model recapitulates many aspects of human-*M. tuberculosis* infection and serves as model to investigate the structural components of the mycobacterial granuloma. Here, we demonstrate that the zebrafish-*M. marinum* granuloma contains foam cells and that transdifferentiation of macrophages into foam cells is driven by the mycobacterial ESX1 pathogenicity locus. Furthermore, we define a detrimental role for infection-induced alterations host lipid metabolism in mycobacterial pathogenesis. Depletion of LDLR, a key regulator of intracellular lipids, decreased *M. marinum* burden and corrected

infection-induced altered lipid metabolism. This resulted reduced macrophage transformation into foam cells within granulomas. Our results demonstrate a conserved role for host lipid metabolism, and specifically the LDL-LDLR axis, in mycobacterial pathogenesis.

Importance

Mycobacterial infections are classically defined by the presence of granulomas at the site of infection. Foams cells are a key component of mycobacterial granulomas and arise as a consequence of local and systemic changes to host lipid metabolism. It is hypothesised that foam cells provide a lipid-rich intracellular environment, promoting mycobacterial survival within the granuloma. Here we have turned to the zebrafish-*M. marinum* platform to identify the host-pathogen interactions contributing to macrophage transdifferentiation into foam cells and the consequences of infection-induced dyslipidemia. We observe foam cells in embryonic and adult zebrafish granulomas, and identify a role for the mycobacterial ESX1 pathogenicity locus in promoting foam cell differentiation. We show that zebrafish-*M. marinum* infection results in dysregulation of host lipid metabolism, and that depletion of the host lipid metabolism node LDLR corrects infection-induced changes to host lipid metabolism and reduces foam cell formation.

Introduction

Mycobacterial manipulation of host lipid metabolism and the transformation of macrophages into foam cells are important pathways in the pathogenesis of *Mycobacterium tuberculosis* (*Mtb*) infection (1). Mycobacteria drive the transformation of infected macrophages into foam cells through the imbalance of low density lipoprotein (LDL) influx and efflux mechanisms (2). Given the significant proportion of the mycobacterial genome that is allocated to lipid metabolism, and the utilisation of lipids such as cholesterol for growth *in vitro*, the abundance

of neutral lipids contained within the granuloma microenvironment may supply a carbon source for intracellular mycobacterial survival and persistence (3).

Dyslipidaemia and foam cell differentiation are known to contribute to disease pathology and prognosis in human *Mtb* infection where foamy macrophages may inhibit lymphocyte access to infected macrophages, increase the build-up of caseum at the center of granulomas, and provide lipids utilized during evasion of phagocytosis (4, 5). However, the involvement of foam cells and dyslipidemia in the pathogenesis of non-tubercular mycobacterial infections, such as *Mycobacterium avium* subspecies *paratuberculosis* (MAP) or *Mycobacterium marinum*, has not been explored. Our group has identified infection-induced changes to host lipid metabolism genes in MAP-infected cattle and aberrant host lipid metabolism gene expression and intracellular cholesterol accumulation within MAP-infected macrophages (6, 7). Here, we have turned to the natural host-pathogen pairing of the zebrafish-*M. marinum* platform to investigate the conservation and consequences of altered host lipid metabolism as a conserved motif across mycobacterial infections.

Zebrafish (*Danio rerio*) are a powerful animal model to study early host-pathogen interactions. Zebrafish demonstrate a functional innate immune system from early in embryogenesis with a high degree of homology to mammals (8). *M. marinum* is a natural pathogen of fish and amphibian species and genomic analysis has identified *M. marinum* as the closest genetic relative of the *Mtb* complex, sharing 85% of orthologous regions with *Mtb* (9). Zebrafish models of *M. marinum* infection have provided unique insight into host-pathogen interplay responsible for granuloma formation, exquisitely reproducing the cellular structure of the human-*M. tuberculosis* granulomas (10-12). As such, the zebrafish-*M. marinum* model is an important platform for investigating immunopathogenesis of the

mycobacterial granuloma, providing fundamental insights into the role of macrophage epithelial transdifferentiation in granuloma maturation (10).

The aim of this study was to explore the biological significance of infection-induced lipid metabolism in a model non-tubercular mycobacterial infection. Our findings demonstrate the key lipid metabolism node, Low Density Lipoprotein Receptor (LDLR), mediates the uptake of lipids into the mycobacterial granuloma niche and aids the transformation of macrophages into foam cells.

Results

Lipid accumulation is observed in adult zebrafish-*M. marinum* granulomas

Adult zebrafish infected with *M. marinum* form highly organized and caseous necrotic granulomas that recapitulate many important aspects of the human-*M. tuberculosis* granuloma (10, 11). To determine if lipids accumulated in these complex zebrafish-*M. marinum* granulomas, adult zebrafish (>3 months old) were infected by intraperitoneal injection of *M. marinum* and maintained for 2 weeks post-infection, a time point where the animals contain a mixture of cellular and necrotic granulomas (11, 12). Strong Oil Red O staining was observed in the cellular layer of necrotic granulomas and weaker Oil Red O staining was observed throughout cellular granulomas (Figure 1A and 1B).

The finding that detectable foam cells correlate with granuloma maturation is consistent with their proposed role in granuloma immunopathology (4). We hypothesize granuloma lipid accumulation correlates with maturation and the progression to necrotic granulomas. To investigate this hypothesis, we used the zebrafish embryo to characterize the genesis of foam cells through temporal and functional analyses.

Lipid accumulation is observed in zebrafish embryo-*M. marinum* granulomas

Zebrafish embryos lack an adaptive immune system and form simple *M. marinum*-containing granulomas primarily consisting of macrophages (10). These simple granulomas have demonstrated remarkable immunopathology fidelity to more complicated adult zebrafish and mammalian granulomas (10-13). We investigated the temporal relationship of foam cell formation with known stages of granuloma maturation in the embryo model. Embryos were individually imaged for fluorescent mycobacterial distribution and stained with Oil Red O at 4 and 6 days post-infection (dpi). Granuloma lipid accumulation was first observed at 4 dpi and was increased in intensity at 6 dpi (Figures 1C and 1D).

Consistent with the Oil Red O staining pattern in adult granulomas, the appearance of putative foam cells in the embryo granulomas correlated with granuloma maturation and was markedly increased at a timepoint when there is significant granuloma necrosis.

Foam cell formation is driven by mycobacterial pathogenesis

To establish if *M. marinum* drives foam cell transdifferentiation as a part of its granuloma-inducing pathogenic program, we infected zebrafish embryos with Δ*ESX1 M. marinum*. The ΔESX1 mutant strain is able to persist and multiply in zebrafish embryos, however it drives granuloma maturation to a much lesser degree than the parental strain (13, 14). Compared to burden-matched embryos infected with WT *M. marinum*, Δ*ESX1*-infected larvae showed significantly less Oil Red O staining in mycobacterial granulomas (Figures 2A and 2B).

This experiment suggests foam cell genesis is driven by pathogenic mycobacteria as part of the ESX-1 virulence program. Taken with the circumstantial evidence that foam cells provide

a niche for mycobacterial growth and a haven from antibiotics and immune killing, these data suggest mycobacteria manipulate host lipid metabolism to drive transdifferentiation of permissive foam cells.

Infection-induced altered host dislipidemia is recapitulated in the zebrafish-*M. marinum* infection model

Previous reports have identified hypercholesterolemia as a correlate of disease pathology during human *Mtb* infection (5). To determine whether these findings were conserved within the zebrafish-*M. marinum* platform, we infected zebrafish embryos with *M. marinum* then analysed the total embryo LDL and HDL content at 3 and 5 dpi, corresponding to an early infection timepoint and the onset of granuloma necrosis, respectively. Calculation of lipoprotein content revealed a skewing towards LDL demonstrating conservation of the infection-induced dyslipidemia phenotype in our zebrafish embryo model (Figure 3A).

Knockdown of *Ldlra* reduces *M. marinum* burden in zebrafish embryos

Infection of macrophages with various species of mycobacteria, including in the zebrafish-*M. marinum* system, increases *LDLR* transcription (6, 15). Given the infection-induced changes in the ligand LDL in our model, we tested the functional relevance of LDLR by morpholino knockdown of the zebrafish *ldlra* gene (16). Depletion of Ldlra had no effect on embryo development, and editing of the *ldlra* transcript was confirmed (Figures 3B, S1A and S1B). Oil Red O staining for lipids in Ldlra-depleted embryos revealed marked vascular lipid accumulation consistent with previous reports of Ldlra depletion being atherogenic (Figure S1C) (16).

Following Ldlra-depletion, embryos were infected with fluorescent *M. marinum* and bacterial burden was analysed by fluorometry. Zebrafish embryos depleted of Ldlra displayed a significantly decreased bacterial burden at 3 and 5 dpi when compared to control embryos (Figures 3C, 3D, S2A and S2B).

Knockdown of Ldlra corrects infection-induced altered host lipid metabolism

Host lipid metabolism is a tightly controlled biological pathway, responsible for addressing the cellular lipid requirements through the regulation of influx and efflux mechanisms. Of the many surface receptors involved in lipid metabolism, LDLR is arguably the most important, playing a key role in driving the uptake of circulating LDL (2).

Following *M. marinum* infection, expression of the LDLR-network and lipid efflux gene *ABCA1* was markedly increased (Figure 4A). Depletion of Ldlra significantly reduced *abca1* transcription, demonstrating a transcriptional conservation of infection-induced lipid metabolism network in our model (Figure 4A).

We hypothesised that infection-induced LDLR is a key node in driving infection-induced hyperlipidaemia, and that depletion of LDLR would prevent infection-induced hypercholesterolemia and the accumulation of lipids within granulomas. Following *M. marinum* infection, Ldlra-deficient embryos displayed a decreased LDL:HDL ratio compared to infected controls at 5 dpi (Figure 4B).

Next, we hypothesised that the combination of reduced potential for LDL uptake and correction of total cholesterol levels would reduce granuloma lipid accumulation in Ldlra-depleted embryos. Granuloma Oil Red O lipid staining density was reduced in infected Ldlra-

deficient embryos compared to infected controls demonstrating a functional role for LDLR in directing bacterial-beneficial lipid accumulation during mycobacterial infection (Figures 4C, 4D, S3A and S3B).

Discussion

A hallmark of mycobacterial disease is the formation of granulomas at the site of infection (17). Foam cells are an important histological component of granulomas and their transformation is driven by the dysregulation of macrophage lipoprotein influx and efflux (2). These lipid-filled macrophages are deficient in their phagocytic abilities and provide an intracellular carbon-based nutrition source, enabling the intracellular survival of mycobacteria (2). Our findings in this study demonstrate 1) infection-induced altered host lipid metabolism is a conserved feature of non-tuberculous mycobacterial infection, and 2) host expression of LDLR is co-opted by mycobacterial infection to increase susceptibility to mycobacterial infection.

This is the first report of mycobacterial infection-induced foam cells in the zebrafish model and recapitulates an important histological correlate of human TB disease in this important model organism. Our results show foam cell transdifferentiation is a correlate of granuloma maturation and that this accumulation of lipids in the granuloma is part of a highly conserved mycobacterial pathogenicity program. Our findings demonstrate the zebrafish-*M. marinum* platform will be applicable further mechanistic studies of infection-induced foam cell transdifferentation.

The elevation of host lipids following mycobacterial infection has been well documented in both human and murine *Mtb* infections (5, 18). Recently, we have shown that elevated serum

cholesterol is associated with histopathological lesions in sheep and cattle infected with MAP (19). The results from the current study are in agreement with previous findings and suggest that the induction of host hypercholesterolemia is a conserved motif of pathogenic mycobacteria. Furthermore, our results demonstrated that *ldlr* knockdown significantly altered the availability of circulating lipoproteins and decreased Oil Red O staining density, providing strong evidence to suggest that the abundance of neutral lipids and therefore foam cells, was largely decreased as a consequence of *ldlr* depletion.

Host lipid metabolism is a complex pathway involving many transcription factors, surface molecules and feedback mechanisms. In the absence of key components, compensatory pathways are utilised to achieve cellular homeostasis. Expression of *abca1* was increased following *M. marinum* infection, in agreement with previous studies identifying the upregulation of *ABCA1* by mycobacterial infection across multiple host species (20). Interestingly, there was a notably lower expression in *ldlra*-deficient embryos, presumably due to the decreased efflux of lipids from mycobacteria-infected macrophages as a consequence of the altered lipoprotein abundance.

Collectively, this study provides evidence of conserved infection-induced altered host lipid metabolism in the zebrafish-*M. marinum* model, and highlights a crucial role of *LDLR* in infection susceptibility across host and pathogen species.

Materials and Methods

Zebrafish maintenance and breeding

Adult zebrafish were housed at the Garvan Institute of Medical Research Biological Testing Facility (St Vincent's Hospital AEC Approval 1511) and housed for infection experiments at

the Centenary Institute (Sydney Local Health District AEC Approval 2016-037). Zebrafish embryos were obtained by natural spawning and embryos were raised at 28°C in E3 media.

Morpholino design and microinjection

Splice-blocking morpholino oligonucleotide for *LDLR* (gene variant *ldlra*) was designed from Ensembl transcript sequences (http://www.ensembl.org/index.html) and purchased from Gene Tools. The *LDLR* morpholino (5'-ATCACATTTCATTTCTTACAGCAGT-3') was targeted at the exon 4/intron 4 and 5 splice junction that was expected to cause the excision of exon 4. The control morpholino (5'-CCTCTTACCTCAGTTACAATTTATA-3') is a negative control targeting a human beta-globin intron known to cause no phenotype variations in zebrafish. Embryos at the 1-4 cell stage were injected with 2 nL of morpholino into the yolk. Embryos were raised at 28°C in E3 media.

Infection of adult zebrafish

Adult zebrafish, between the ages of 3 months and 12 months, were infected with approximately 200 CFU *M. marinum* by intraperitoneal injection as previously described (11). Infected animals were recovered into 1 g/L salt water, then fed and monitored daily.

Histological processing of adult zebrafish

Adult zebrafish were euthanized by anesthetic overdose at 2 weeks post-infection and fixed in 10% neutral buffered formalin for 2 days at 4°C. Fixed specimens were washed in PBS, 30% (w/v) sucrose, 50:50 solution of 30% sucrose and OCT, and a final wash in OCT before freezing. 20 microns sections were cut on a Leica cryostat. Slides were refixed in 10% neutral buffered formalin, rinsed in propylene glycol, stained in 0.5% (w/v) Oil Red O dissolved in propylene glycol and counterstained with a 1% (w/v) solution of methylene blue.

Infection of zebrafish embryos

At 30 hours post-fertilisation, zebrafish embryos were anaesthetised with 160 µg/mL tricaine (Sigma-Aldrich) and infected with approximately 200 CFU M strain *M. marinum* via caudal vein injection. A dose of approximately 1000 CFU Δ*ESX1 M. marinum* was injected to match parental strain burden at 5 dpi.

Oil Red O staining

Oil Red O lipid staining on whole mount embryos was completed as previously described (21). Briefly, embryos were individually imaged for bacterial distribution by fluorescent microscopy, fixed, and stained in Oil Red O (0.5% w/v in propylene glycol). Oil Red O staining intensity at sites of infection were quantified in ImageJ and calculated as the pixel density above background tissue.

Imaging

Live zebrafish embryos were anaesthetized in M-222 (Tricaine) and mounted in 3% methylcellulose for imaging on a Leica M205FA fluorescence stereomicroscope. Histological sections were imaged on a Leica DM6000B. Further image manipulation and/or bacterial quantification was carried out with Image J Software Version 1.51j.

Quantification of *M. marinum* burden by fluorescent pixel count

Infection burden was measured as the number of pixels in each embryo above background fluorescence in ImageJ (National Institutes of Health) and pixels counted using the ‘Analyse particles’ function (22).

Lipoprotein assay

Lipoprotein abundance was measured using the HDL & LDL/VLDL Cholesterol Assay Kit (Cell Biolabs) as per manufacturer's instructions and based on previously published methods (16). Briefly, 10 embryos per treatment group were terminally anaesthetised and placed into BHT solution (10 µg/mL, Sigma-Aldrich) and homogenised. Homogenates were centrifuged at 4°C at 2000 *g* for 5 mins to pellet debris. The supernatant was mixed with an equal volume of precipitation solution to separate the high density lipoprotein (HDL) and low density lipoprotein (LDL) fractions. Each lipoprotein fraction was mixed with an equal volume of reaction mix and quantified by fluorescent plate reader. A standard curve was included in each run to calculate the concentration of lipoproteins within each treatment.

Molecular analysis of *ldlra* knockdown

RNA was extracted in TRIZOL (Thermofisher) by precipitation and cDNA was synthesised with an Applied Biosystems High Capacity cDNA reverse transcription kit (Thermofisher). PCR was performed with *ldlra*-specific primers (5'-AGAGCTGGAAATGTGACGGA-3' and 3'-CTCATCTGGACGGCATGTTG-5') and visualised by gel electrophoresis.

Quantitative PCR

Quantitative PCR (qPCR) reactions were completed as previously described (23) using Mx3000P real-time PCR systems (Stratagene). Gene-specific primers were generated for *abca1* (5'-AGCTGCTGGTCGAGATCATA-3' and 3'- CTGTCTCACTGCATGCTTGG-5') for comparison against housekeeping gene *actb* (5'-CCTTCCAGCAGATGTGGATT-3' and 3'-CACCTTCACCGTTCCAGTTT-5'). Samples were run in duplicate with reaction specificity confirmed based on the post-amplification dissociation curve.

Statistical analysis

Prism (Graphpad) was used to perform statistical testing as indicated by unpaired Student's t-tests and ANOVA.

Acknowledgements

This work was supported by the Australian National Health and Medical Research Council (APP1099912 and APP1053407 to S.H.O.); Meat and Livestock Australia (P.PSH. 0813 to A.C.P. and K. dS); the Marie Bashir Institute for Infectious Diseases and Biosecurity (grant to S.H.O., A.C.P. and K. dS); University of Sydney Fellowship (grant to S.H.O.); and the Kenyon Family Inflammation Award (grant to S.H.O.), Consellería de Economía, Emprego e Industria (GAIN), Xunta de Galicia (grant IN607B 2016/12 to Institute of Marine Research (IIM-CSIC)).

Dr Kristina Jahn and Sydney Cytometry for assistance with imaging. Special thanks goes to the animal house staff at the Garvan Institute of Medical Research and CSIC.

References

1. Lovewell RR, Sassetti CM, VanderVen BC. 2016. Chewing the fat: lipid metabolism and homeostasis during M. tuberculosis infection. Curr Opin Microbiol 29:30-6.
2. Cardona P, Allain S, Altare F, Kim M, Russell DG. 2009. Foamy macrophages and the progression of the human tuberculosis granuloma. Nature Immunology 10:943-948.
3. Pandey AK, Sassetti CM. 2008. Mycobacterial persistence requires the utilization of host cholesterol. Proceedings of the National Academy of Sciences of the United States of America 105:4376-4380.

4. Russell DG, Cardona PJ, Kim MJ, Allain S, Altare F. 2009. Foamy macrophages and the progression of the human tuberculosis granuloma. Nat Immunol 10:943-8.

5. Dong Z, Shi J, Dorhoi A, Zhang J, Soodeen-Lalloo AK, Chen W, Yin H, Sha W, Li W, Zheng R, Liu Z, Yang H, Qin L, Wang J, Huang X, Wu C, Kaufmann SHE, Feng Y. 2017. Hemostasis and Lipoprotein Indices Signify Exacerbated Lung Injury in Tuberculosis With Diabetes Comorbidity. Chest doi:10.1016/j.chest.2017.11.029.

6. Johansen MD, de Silva K, Plain KM, Whittington RJ, Purdie AC. submitted. *Mycobacterium avium* subspecies *paratuberculosis* is able to manipulate host lipid metabolism and accumulate cholesterol within macrophages. Pathogens and Disease.

7. Thirunavukkarasu S, de Silva K, Plain KM, Whittington RJ. 2014. Role of host- and pathogen-associated lipids in directing the immune response in mycobacterial infections, with emphasis on Mycobacterium avium subsp. paratuberculosis. Critical reviews in microbiology doi:10.3109/1040841X.2014.932327:1-13.

8. Traver D, Herbomel P, Patton EE, Murphey RD, Yoder JA, Litman GW, Catic A, Amemiya CT, Zon LI, Trede NS. 2003. The Zebrafish as a Model Organism to Study Development of the Immune System. Advances in Immunology 81:253-330.

9. Stinear TP, Seemann T, Harrison PF, Jenkin GA, Davies JK, Johnson PDR, Abdellah Z, Arrowsmith C, Chillingworth T, Churcher C, Clarke K, Cronin A, Davis P, Goodhead I, Holroyd N, Jagels K, Lord A, Moule S, Mungall K, Norbertczak H, Quail MA, Rabbinowitsch E, Walker D, White B, Whitehead S, Small PLC, Brosch R, Ramakrishnan L, Fischbach MA, Parkhill J, Cole ST. 2008. Insights from the complete genome sequence of *Mycobacterium marinum* on the evolution of *Mycobacterium tuberculosis*. Genome Research 18:729-741.

10. Cronan MR, Beerman RW, Rosenberg AF, Saelens JW, Johnson MG, Oehlers SH, Sisk DM, Jurcic Smith KL, Medvitz NA, Miller SE, Trinh LA, Fraser SE, Madden JF,

Turner J, Stout JE, Lee S, Tobin DM. 2016. Macrophage Epithelial Reprogramming Underlies Mycobacterial Granuloma Formation and Promotes Infection. Immunity 45:861-876.

11. Oehlers SH, Cronan MR, Scott NR, Thomas MI, Okuda KS, Walton EM, Beerman RW, Crosier PS, Tobin DM. 2015. Interception of host angiogenic signalling limits mycobacterial growth. Nature 517:612-5.

12. Oehlers SH, Cronan MR, Beerman RW, Johnson MG, Huang J, Kontos CD, Stout JE, Tobin DM. 2017. Infection-induced vascular permeability aids mycobacterial growth. J Infect Dis 215:813-7.

13. Davis JM, Ramakrishnan L. 2009. The role of the granuloma in expansion and dissemination of early tuberculous infection. Cell 136:37-49.

14. Volkman HE, Pozos TC, Zheng J, Davis JM, Rawls JF, Ramakrishnan L. 2010. Tuberculous granuloma induction via interaction of a bacterial secreted protein with host epithelium. Science 327:466-9.

15. Kim MJ, Wainwright HC, Locketz M, Bekker LG, Walther GB, Dittrich C, Visser A, Wang W, Hsu FF, Wiehart U, Tsenova L, Kaplan G, Russell DG. 2010. Caseation of human tuberculosis granulomas correlates with elevated host lipid metabolism. EMBO Molecular Medicine 2:258-74.

16. O'Hare EA, Wang X, Montasser ME, Chang YC, Mitchell BD, Zaghloul NA. 2014. Disruption of ldlr causes increased LDL-c and vascular lipid accumulation in a zebrafish model of hypercholesterolemia. Journal of lipid research 55:2242-2253.

17. Ramakrishnan L. 2012. Revisiting the role of the granuloma in tuberculosis. Nature Reviews Immunology 12:352-366.

18. Martens GW, Arikan MC, Jinhee L, Ren F, Vallerskog T, Kornfeld H. 2008. Hypercholesterolemia Impairs Immunity to Tuberculosis. Infection and Immunity 76:3464-3472.

19. Johansen MD, De Silva K, Plain KM, Begg DJ, Whittington RJ, Purdie AC. submitted. Sheep and cattle exposed to *Mycobacterium avium* subspecies *paratuberculosis* exhibit altered total serum cholesterol profiles during the early stages of infection. Veterinary Immunology and Immunopathology.

20. Long J, Roy RB, Zhang YJJ, Antrobus R, Du YX, Smith DL, Weekes MP, Javid B. 2016. Plasma Membrane Profiling Reveals Upregulation of ABCA1 by Infected Macrophages Leading to Restriction of Mycobacterial Growth. Frontiers in Microbiology 7:1086-1097.

21. Passeri MJ, Cinaroglu A, Gao C, Sadler KC. 2009. Hepatic steatosis in response to acute alcohol exposure in zebrafish requires sterol regulatory element binding protein activation. Hepatology 49:443-52.

22. Matty MA, Oehlers SH, Tobin DM. 2016. Live Imaging of Host-Pathogen Interactions in Zebrafish Larvae. Methods Mol Biol 1451:207-23.

23. Taylor DL, Zhong L, Begg DJ, de Silva K, Whittington RJ. 2008. Toll-like receptor genes are differentially expressed at the sites of infection during the progression of Johne's disease in outbred sheep. Veterinary Immunology and Immunopathology 124:132-151.

Figure Legends

Figure 1: Lipid accumulation is present within the granulomas of zebrafish adults and embryos infected with *M. marinum*.

A, Oil Red O staining of a necrotic granuloma from an adult zebrafish infected with *M. marinum* at 2 weeks post-infection. *B*, Oil Red O staining of a cellular granuloma from an adult zebrafish infected with *M. marinum* at 2 weeks post-infection. Note the heavier Oil Red O staining in the necrotic granuloma. Scale bars represent 100 µm. *C*, Representative images of Oil Red O staining density at 4 and 6 days post-infection. Red circles indicate areas of embryos with largest foci of infection. Scale bars represent 500 µm. *D*, Quantification of Oil Red O staining density of granulomas in zebrafish embryos at 4 and 6 days post-infection. Each data point represents the Oil Red O staining density of an individual granuloma. Error bars represent standard deviation, statistical tests were performed using an unpaired T-test.

Figure 2: Granuloma lipid accumulation is driven by mycobacterial pathogenicity locus ESX1.

A, Representative images of Oil Red O staining in zebrafish embryos infected with wild-type or ΔESX1 *M. marinum* at 5 days post-infection. Red circles indicate areas of embryos with largest foci of infection. Scale bars represent 500 µm. *B*, Quantification of Oil Red O density units in embryos infected with wild-type or ΔESX1 *M. marinum*. Each data point represents an individual granuloma. Error bars represent standard deviation. Analysis of Oil Red O density units was completed using an unpaired Student's *t*-test.

Figure 3: LDL is increased by infection and knockdown of Ldlra reduces *M. marinum* bacterial burden.

A, Quantification of LDL concentration in wild-type zebrafish embryos at 5 days following *M. marinum* infection. Each data point represents a pooled sample of 10 embryos. *B*, Molecular validation of *ldlra* morpholino efficacy at 3 and 5 days post-treatment. *C*, Representative images of *M. marinum*-wasabi bacterial distribution at 5 days-post infection. Scale bar represents 500 µm. *D*, Quantification of *M. marinum* bacterial burden by fluorometry at 5 days post-infection. Error bars represent standard deviations. Each data point represents an individual embryo. Statistical tests were performed using unpaired Student's t-tests. Experiments were completed with 4 independent biological replicates for each panel.

Figure 4: Mycobacterial infection-induced modulation of host lipid metabolism is corrected in Ldlra-deficient embryos.

A, *abca1* transcript fold change expression at 5 days post-infection measured by qPCR. Each column represents two independent biological replicates completed with technical replicates. *B*, Quantification of LDL concentration in Ldlra-deficient embryos at 5 days-post infection. Each data point represents a pooled sample of 10 embryos completed with four independent replicates. *C*, Representative images of Oil Red O staining density at 5 days post-infection. Red circles indicate areas of embryos with largest foci of infection. Scale bar represents 500 µm. *D*, Quantification of granuloma Oil Red O staining density units at 5 days post-infection. Each data point represents an individual granuloma. Error bars represent standard deviation. Gene expression analysis was completed using one-way ANOVA. Statistical tests were completed using unpaired Student's *t*-tests.

Supplementary figure 1: Knockdown of Ldlra results in extensive lipid accumulation with the vasculature.

A, Normal morphology and phenotypes at 5 days post-fertilisation. *B*, Embryos deficient in Ldlra show normal phenotypes at 5 days following morpholino treatment. *C*, Embryos deficient in Ldlra display visible lipid abundance within the vasculature following Oil Red O lipid staining. White arrows represent expansive lipid accumulation within the vasculature. Scale bars represent 500 µm.

Supplementary figure 2: Bacterial burden is reduced in Ldlra-deficient embryos at 3 days post-infection.

A, Representative images of *M. marinum* bacterial burden at 3 days-post infection. Scale bars represent 500 µm. Quantification of *M. marinum* bacterial burden at 3 days post-infection. Error bars represent standard deviations. Each data point represents an individual embryo. Analysis of bacterial burden was performed using an unpaired Student's *t*-test. Experiments were completed with 4 independent biological replicates for each panel.

Supplementary figure 3: Granuloma Oil Red O staining is reduced in Ldlra-deficient embryos at 3 days post-infection with *M. marinum.*

A, Representative images of Oil Red O staining density at 3 days post-infection with *M. marinum.* Scale bars represent 500 µm. *B*, Quantification of Oil Red O density units at 3 days post-infection with *M. marinum*. Each data point represents an individual granuloma. Error bars represent standard deviation. Statistical tests were performed using an unpaired Student's *t*-test.

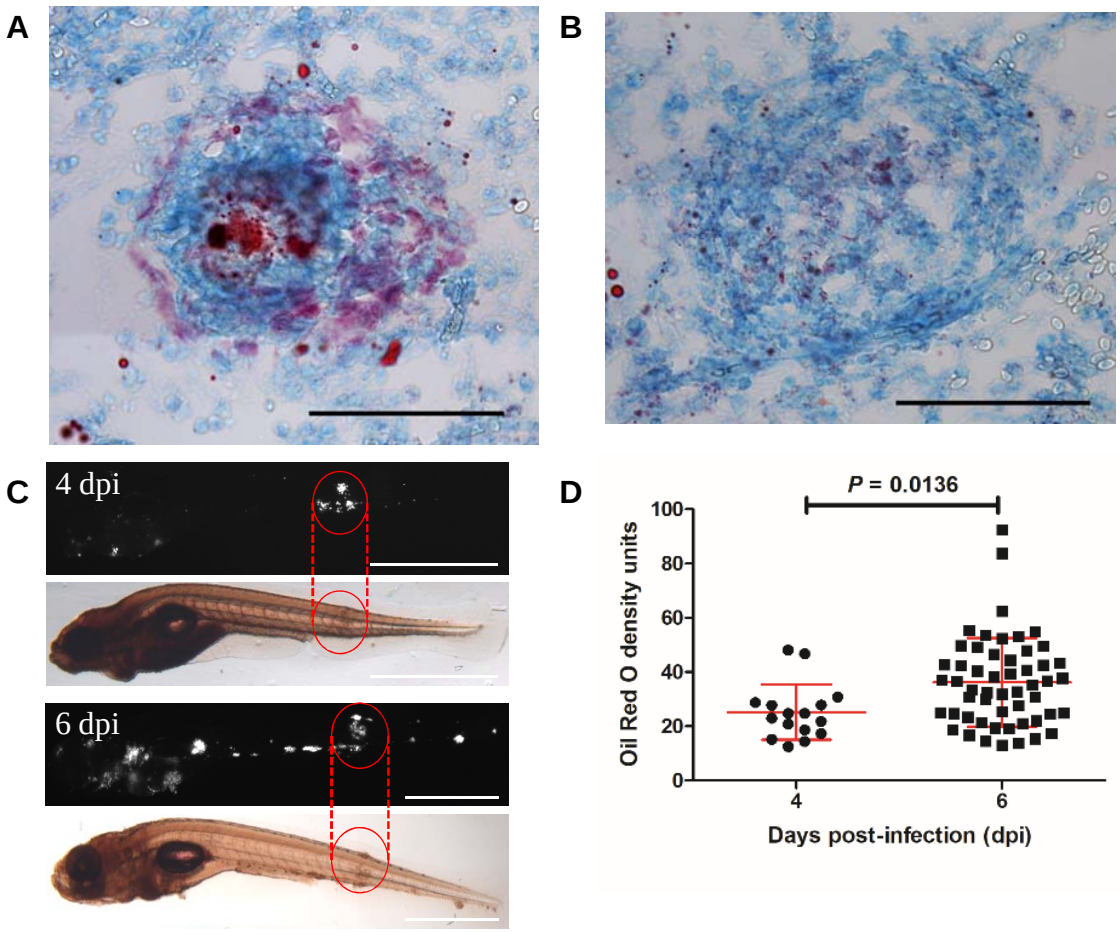

Figure 1: Lipid accumulation is present within the granulomas of zebrafish adults and embryos infected with *M. marinum*.

A, Oil Red O staining of a necrotic granuloma from an adult zebrafish infected with *M. marinum* at 2 weeks post-infection. *B*, Oil Red O staining of a cellular granuloma from an adult zebrafish infected with *M. marinum* at 2 weeks post-infection. Note the heavier Oil Red O staining in the necrotic granuloma. *C*, Representative images of Oil Red O staining density at 4 and 6 days post-infection. Red circles indicate areas of embryos with largest foci of infection. Scale bars represent 500 µm. *D*, Quantification of Oil Red O staining density of granulomas in zebrafish at 4 and 6 days post-infection. Each data point represents the Oil Red O staining density of an individual granuloma. Error bars represent standard deviation, statistical tests were performed using an unpaired T-test.

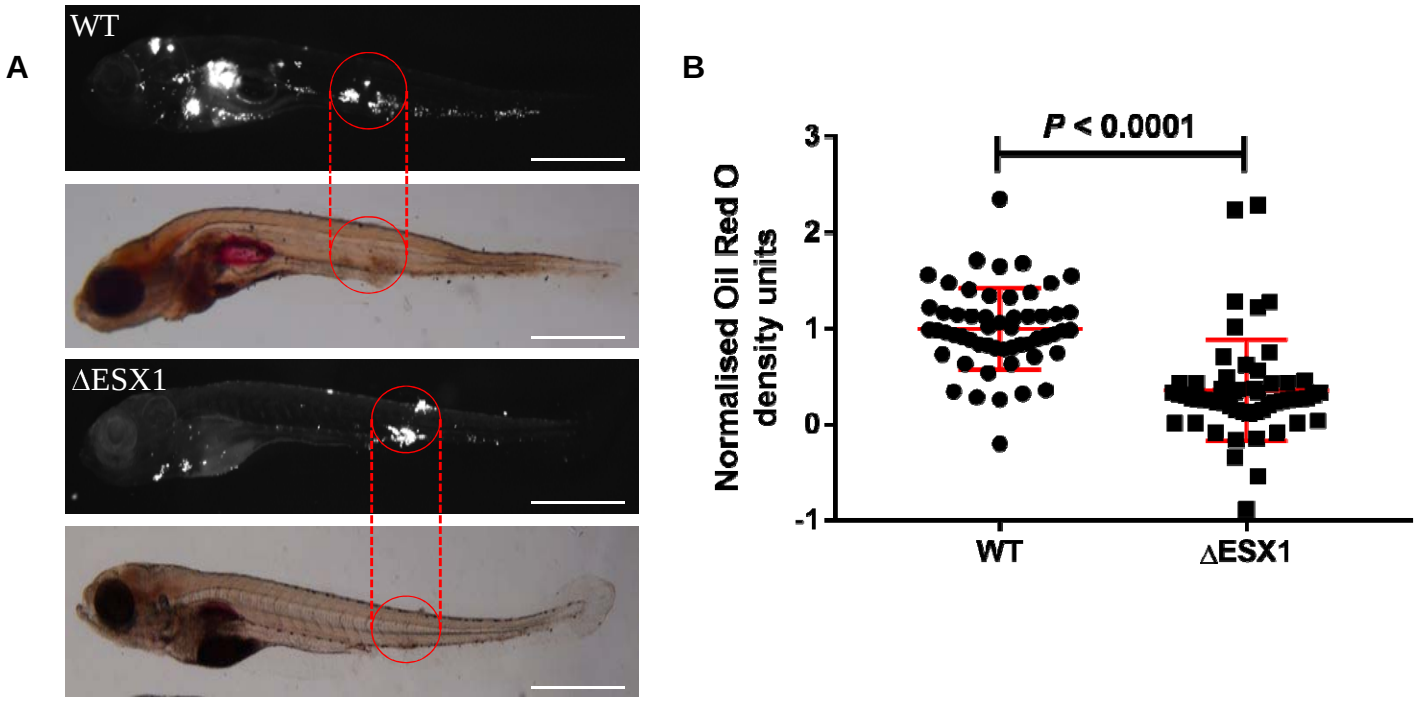

Figure 2: Granuloma lipid accumulation is driven by mycobacterial pathogenicity locus ESX1.
A, Representative images of Oil Red O staining in zebrafish embryos infected with wild-type or ΔESX1 *M. marinum* at 5 days post-infection. Red circles indicate areas of embryos with largest foci of infection. Scale bars represent 500 µm. *B*, Quantification of Oil Red O density units in embryos infected with wild-type or ΔESX1 *M. marinum*. Each data point represents an individual granuloma. Error bars represent standard deviation. Analysis of Oil Red O density units was completed using an unpaired Student's *t*-test.

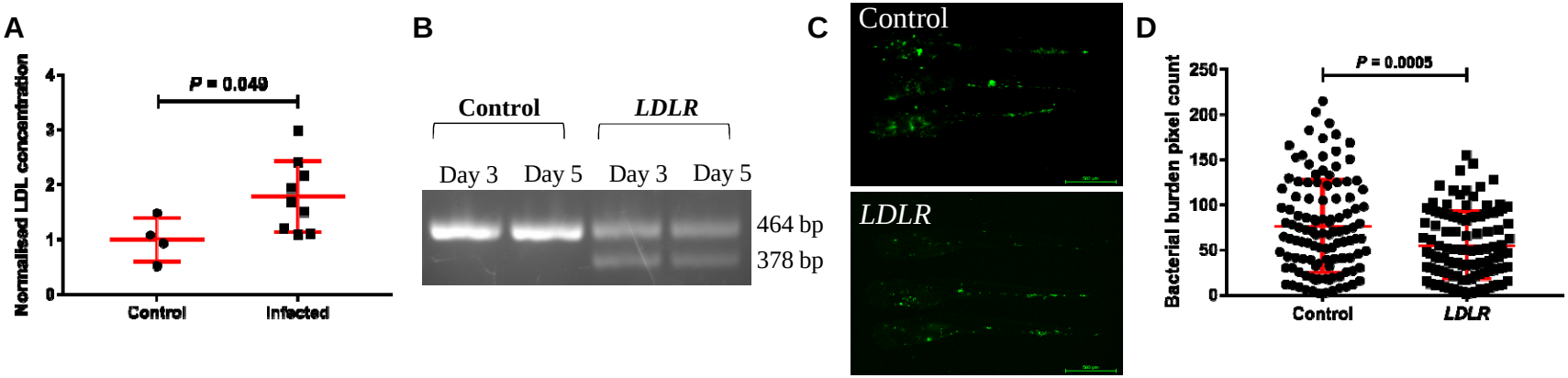

Figure 3: LDL is increased by infection and knockdown of Ldlra reduces *M. marinum* bacterial burden.
A, Quantification of LDL concentration in wild-type zebrafish embryos at 5 days following *M. marinum* infection. Each data point represents a pooled sample of 10 embryos. *B*, Molecular validation of *ldlra* morpholino efficacy at 3 and 5 days post-treatment. *C*, Representative images of *M. marinum*-wasabi bacterial distribution at 5 days-post infection. Scale bar represents 500 µm. *D*, Quantification of *M. marinum* bacterial burden by fluorometry at 5 days post-infection. Error bars represent standard deviations. Each data point represents an individual embryo. Statistical tests for LDL quantification were performed using unpaired Student's t-tests. Analysis of bacterial burden was performed using an unpaired Student's *t*-test. Experiments were completed with 4 independent biological replicates for each panel.

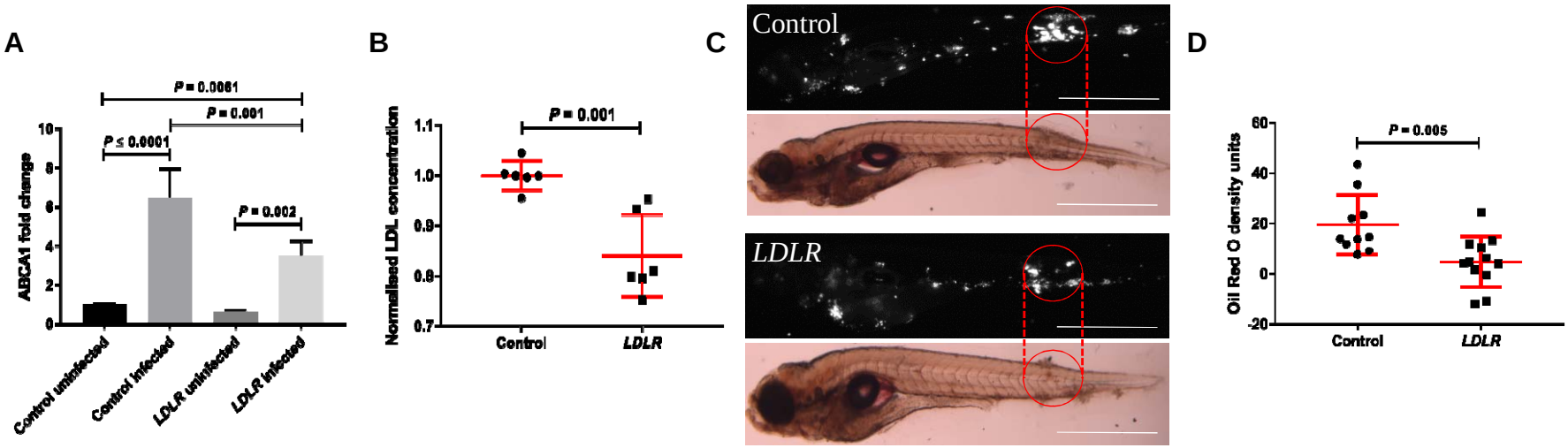

Figure 4: Mycobacterial infection-induced modulation of host lipid metabolism is corrected in Ldlra-deficient embryos.

A, *abca1* transcript fold change expression at 5 days post-infection measured by qPCR. Each column represents two independent biological replicates completed with technical replicates. *B*, Quantification of LDL concentration in Ldlra-deficient embryos at 5 days-post infection. Each data point represents a pooled sample of 10 embryos completed with four independent replicates. *C*, Representative images of Oil Red O staining density at 5 days post-infection. Red circles indicate areas of embryos with largest foci of infection. Scale bar represents 500 µm. *D*, Quantification of granuloma Oil Red O staining density units at 5 days post-infection. Each data point represents an individual granuloma. Error bars represent standard deviation. Gene expression analysis was completed using one-way ANOVA. Analysis of LDL concentration and Oil Red O density units was completed using an unpaired Student's *t*-test.

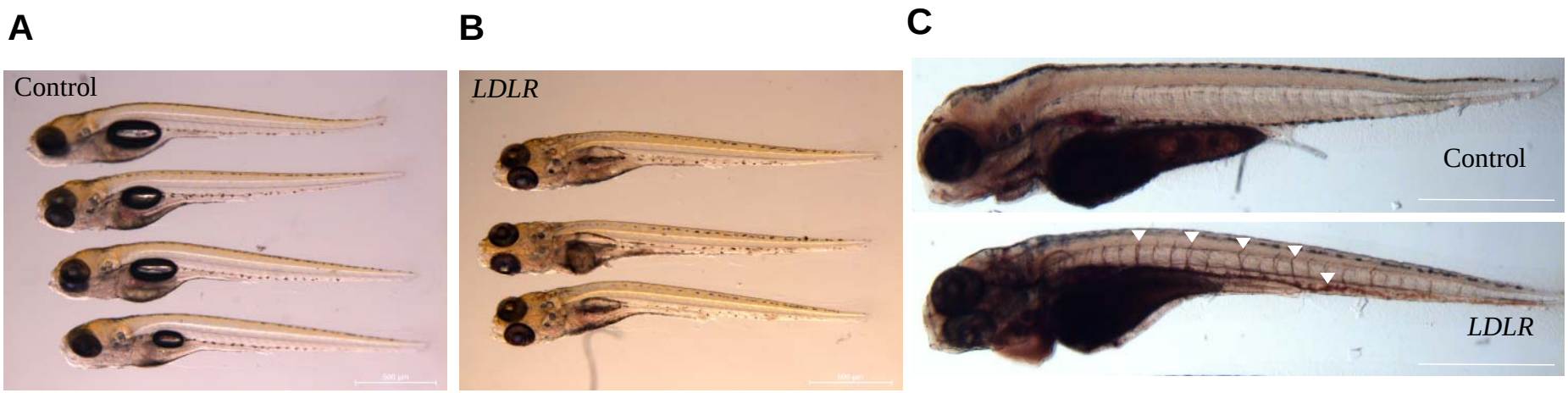

Supplementary figure 1: Knockdown of Ldlra results in extensive lipid accumulation with the vasculature. *A*, Normal morphology and phenotypes at 5 days post-fertilisation. *B*, Embryos deficient in Ldlra show normal phenotypes at 5 days following morpholino treatment. *C*, Embryos deficient in Ldlra display visible lipid abundance within the vasculature following Oil Red O lipid staining. White arrows represent expansive lipid accumulation within the vasculature. Scale bars represent 500 µm.

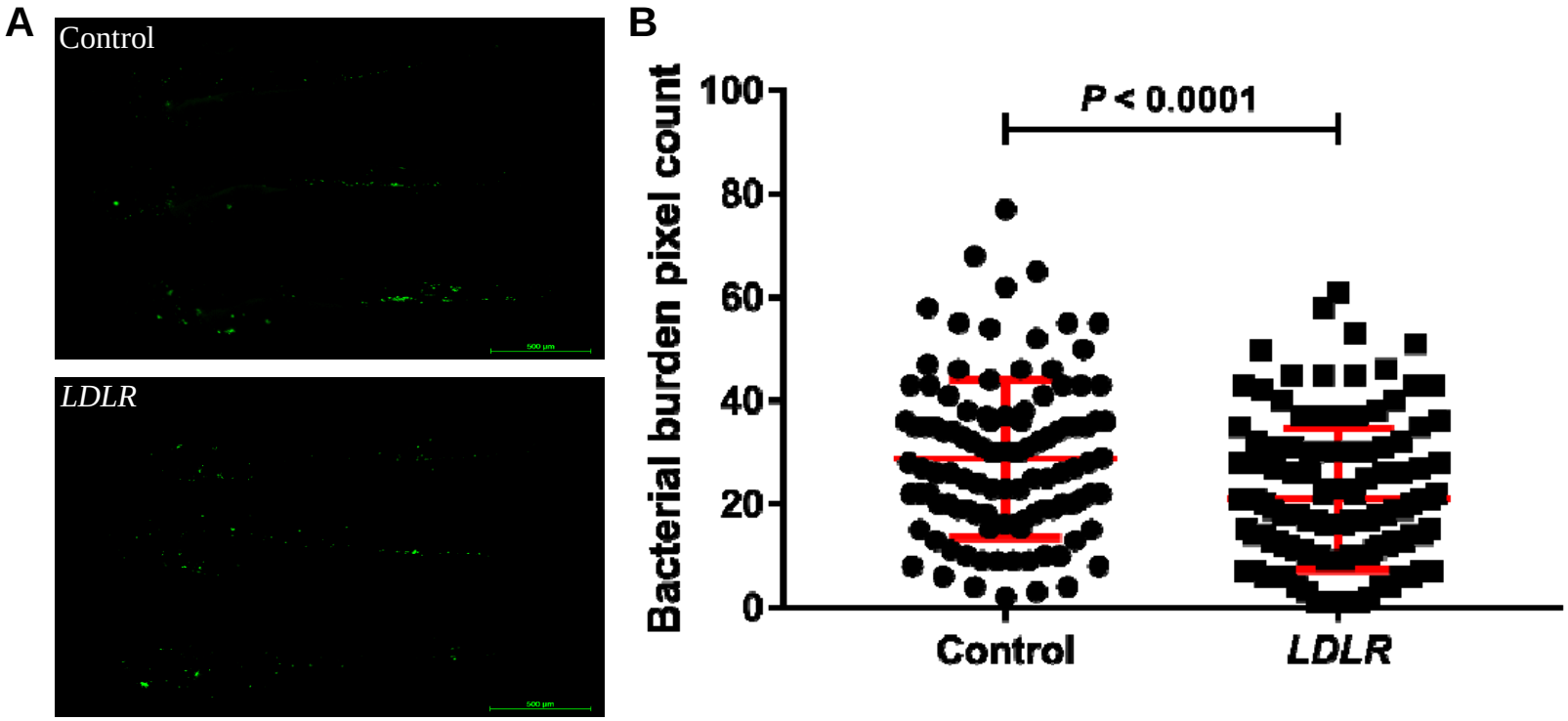

Supplementary figure 2: Bacterial burden is reduced in Ldlra-deficient embryos at 3 days post-infection.
A, Representative images of *M. marinum* bacterial burden at 3 days-post infection. Scale bars represent 500 µm.
Quantification of *M. marinum* bacterial burden at 3 days post-infection. Error bars represent standard deviations.
Analysis of *M. marinum* bacterial burden was completed using REML coupled with Fisher's protected LSD; experiment number was included as random effect.

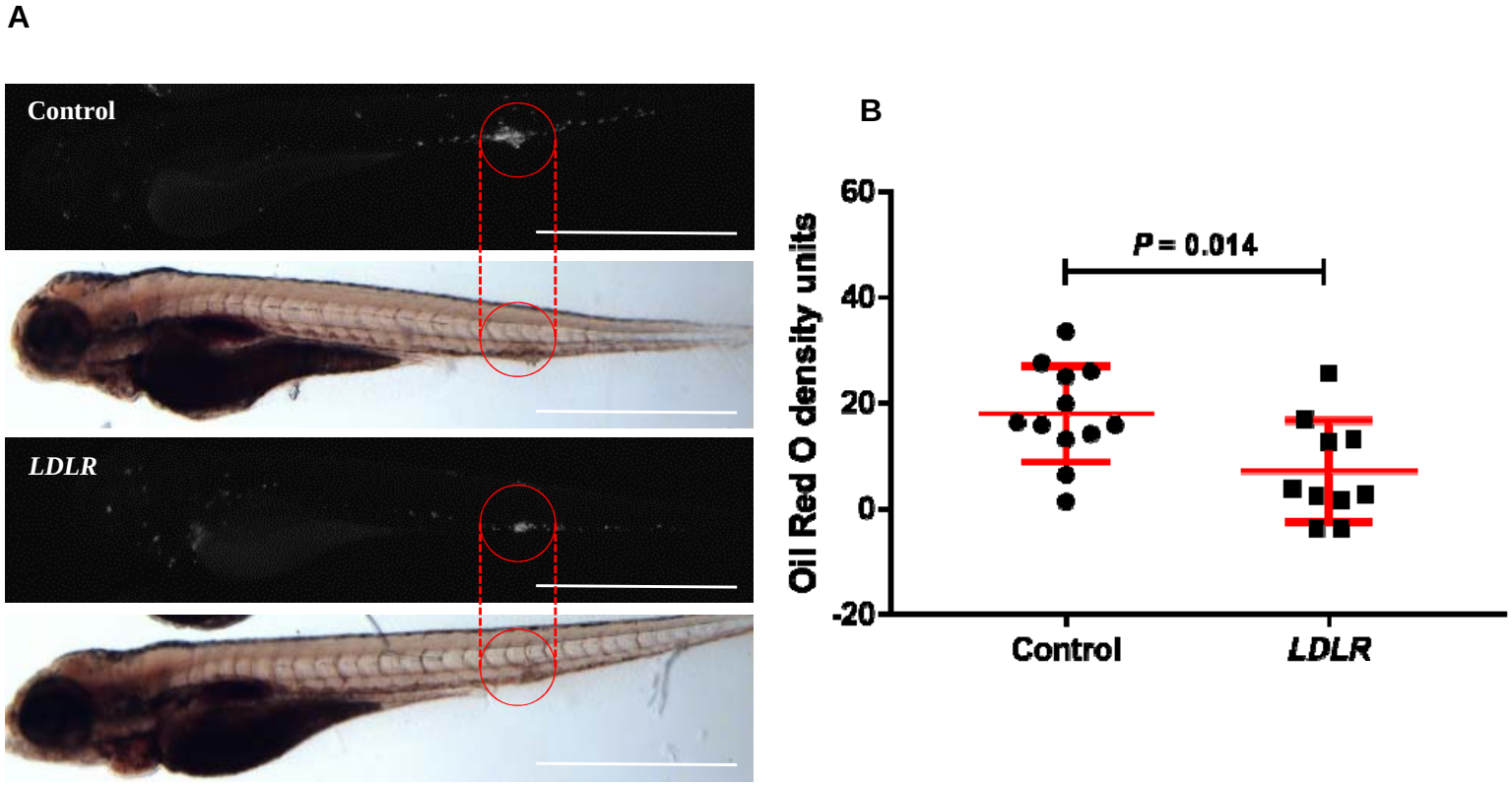

Supplementary figure 3: Granuloma Oil Red O staining is reduced in Ldlra-deficient embryos at 3 days post-infection with *M. marinum*.

A, Representative images of Oil Red O staining density at 3 days post-infection with *M. marinum.* Scale bars represent 500 µm. *B*, Quantification of Oil Red O density units at 3 days post-infection with *M. marinum*. Each data point represents an individual embryo. Error bars represent standard deviation. Statistical tests were performed using unpaired Student's t-tests.